

Magnetohydrostatic (MHS) atmospheres

Laurence J. November

The Light Physics, La Luz NM 88337-0217 USA

August 29, 2003

Abstract. We show that the atmospheric and magnetic height variations are coupled in all MHS equilibria with gravity if isolated thin non-force-free flux tubes are present. In gas-dominated environments, as in stellar photospheres, flux tubes expand rapidly with height to maintain pressure balance with the cool surroundings. But in magnetically dominated environments, as in stellar coronae, the large-scale background magnetic field determines the average spreading of embedded flux tubes, and rigidly held flux tubes *require* a specific surrounding atmosphere with a unique temperature profile for equilibrium. The solar static equilibrium atmosphere exhibits the correct transition-region properties and base coronal temperature for the sun's main magnetic spherical harmonic. Steady flows contribute to the overall pressure, so equilibria with accelerated wind outflows are possible as well. Flux tubes reflect a mathematical degeneracy in the form of non-force-free fields, which leads to coupling in general equilibrium conditions. The equilibrium state characterizes the system average in usual circumstances and dynamics tend to maintain the MHS atmosphere. Outflows are produced everywhere external to flux tubes that refill a depleted or cool atmosphere to the equilibrium gas profile, heating the gas compressively.

Key words. magnetohydrodynamics (MHD) – Sun:magnetic fields – Sun:atmosphere – Sun:corona – Sun:transition region

1. Introduction

In our observation of solar ‘threads’ (November & Koutchmy 1996 or NK96) we puzzled over whether coronal flux tubes should expand with height to maintain pressure balance with the ambient gas-pressure decrease or follow the lines of the external magnetic field. After all, if the corona is independently heated, the gas and magnetic height variations should be generally different. The many observations of EUV and X-ray loops as well as the purely density-sensitive observations of white-light > 15 Mm ‘voids’ (MacQueen et al., 1974), > 2 Mm threads, and scintillation > 1 km filamentary microstructure (Coles & Harmon, 1978; Woo et al., 1995) all suggest that the large-scale solar coronal magnetic field is interspersed with flux tubes with a great range of sizes. Figure 1 shows dark and bright threads in a square region about a solar radius on a side over the west limb taken with the Canada-France-Hawaii Telescope (CFHT) at the unique total-eclipse opportunity on Mauna Kea on July 11, 1991. The dark and bright threads, which were essentially unchanged over the 4-minute eclipse duration, appear to be aligned and organized in arched and radial surfaces, probably current sheets, overlapping in their projection onto the plane of the sky in the line-of-sight view.

We know that isolated thin flux tubes must expand with height in balance with the ambient gas-pressure decrease. The flux-tube gas-pressure difference, external minus internal, is re-

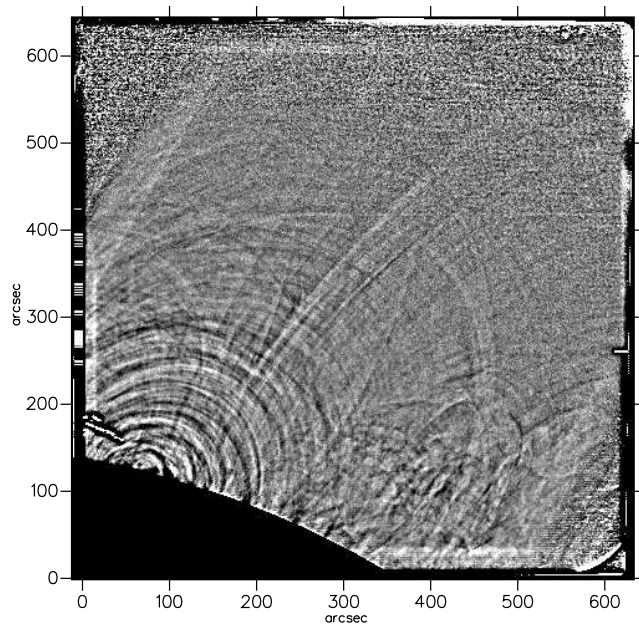


Fig. 1. Unsharp-masked time-averaged white-light eclipse image processed by subtracting a 6 arcsec = 4300 km Gaussian convolution with contrast range $\Delta \ln I = 0.8\%$. Dark and bright threads are probably flux tubes in current sheets.

lated to the magnetic-pressure difference by the static equilibrium relation

$$p_e - p_i = \frac{1}{8\pi} (\mathbf{B}_i^2 - \mathbf{B}_e^2). \quad (1)$$

Correspondence to: nov@thelightphysics.org

The Wilson depression in sunspots shows that at least large-scale photospheric flux tubes are nearly evacuated. Evacuated flux tubes exhibit the maximum magnetic flux concentration and field strength possible. In evacuated flux tubes $p_i = 0$ and the photospheric external field $\mathbf{B}_e = 0$, so the internal field strength must follow the ambient gas-pressure decrease $\mathbf{B}_i(r)^2 = 8\pi p_e(r)$, giving flux tubes that expand with height to conserve their total internal magnetic flux. Since the scale height for $p_e(r)$ is small in the relatively cool photosphere and chromosphere a dramatic flux-tube expansion occurs, which is the accepted explanation for the solar ‘magnetic canopy’ (Giovanelli, 1982). Both voids and a range of sizes of dark threads were also found to have contrasts consistent with what is expected for fully evacuated cylindrical flux tubes (MacQueen et al. 1983; NK96). In the corona, where the external magnetic field is not zero, the magnetic flux inside evacuated flux tubes must decrease with height to follow the total external ambient gas plus magnetic pressures, or $\mathbf{B}_i(r)^2 = 8\pi p_e(r) + \mathbf{B}_e(r)^2$. This gives a small flux-tube expansion with height in the large gas-pressure scale height of the hot corona. A slight flux-tube expansion with height seems evident in some of the threads in figure 1.

We can argue too that the radial expansion of isolated thin flux tubes must conform to the external magnetic field. Parker (1972) showed that

$$(\mathbf{B}_e \cdot \nabla) \mathbf{B}_i = 0, \quad (2)$$

in MHS equilibria without gravity, where \mathbf{B}_e represents a uniform background magnetic field, and the field in flux tubes \mathbf{B}_i contains all of the spatial variations. The theorem is locally applicable everywhere in perturbed MHS equilibria with gravity, i.e. equation (2) with \mathbf{B}_e allowed to vary slowly spatially, as we discuss in §2. Thus thin flux tubes in a gravitational field must spread to follow the lines of the relatively uniform background magnetic field; the radial functional variations must be directly related, that is $|\mathbf{B}_i(r)| \propto |\mathbf{B}_e(r)|$ along flux tubes.

Therefore both ways of looking at the problem are essentially correct. The coronal flux-tube field must comply with the external field $\mathbf{B}_i(r)^2 \propto \mathbf{B}_e(r)^2$, and the radial variation of the external gas pressure outside isolated evacuated coronal flux tubes is proportional to the magnetic-pressure difference $p_e(r) \propto \mathbf{B}_i(r)^2 - \mathbf{B}_e(r)^2$. Hence, the external gas and magnetic pressures must be coupled, $p_e(r) \propto \mathbf{B}_e(r)^2$ outside and along isolated evacuated flux tubes. The background magnetic field is dominant in lower stellar coronae and must determine the expansion of embedded flux tubes. The expansion of evacuated flux tubes then defines the radial variation of the ambient gas pressure for equilibrium, the gas pressure being horizontally stratified in the external force-free or potential field. More generally, flux tubes of arbitrary base pressure but in thermal balance with the local ambient atmosphere satisfy $p_i(r) \propto p_e(r)$, giving the same external atmosphere $p_e(r) \propto \mathbf{B}_e(r)^2$. Thus an atmosphere containing isolated thin non-force-free flux tubes in different forms of local balance must exhibit a temperature profile defined by the dominant background magnetic field for a perfect gas in hydrostatic equilibrium.

The properties of flux tubes reflect a natural degeneracy in the form of non-force-free magnetic fields, and imply the

existence of an underlying *mathematical* relationship between an equilibrium atmosphere and large-scale magnetic field. In §2, we prove that the height variations of the gas pressure and magnetic field amplitude are directly coupled in the most-significant-order terms of the gravitational perturbation in general non-force-free MHS equilibria, with smaller field divergence and curl effects. In low- β systems, with strong magnetic fields, the external gas pressure corresponds to a small difference $p_e(r) = (\mathbf{B}_i(r)^2 - \mathbf{B}_e(r)^2)/(8\pi)$, which allows large pressure deviations for a given relative flexibility of the large-scale magnetic field around individual flux tubes. Magnetic fields can exhibit and persist in significant deviations from equilibrium, however the coupling $p_e(r) \propto \mathbf{B}_e(r)^2$ describes the general equilibrium condition for arbitrary β .

Historical MHS equilibrium solutions with gravity have also suggested that a general relationship exists between the large magnetic and gas-pressure scales. Dungey (1953) derived plane-parallel MHS equilibria for a magnetic field with its degenerate axis directed perpendicular to gravity (see also Low 1975; Cheng & Choe 1998). His solutions are represented in a modified Grad-Shafranov (GS) Equation that retains the gas-pressure radial scale-height variation as a separable factor in the pressure term. Dungey showed that when the magnetic field is also zero in its degenerate axis, the separable factor can be absorbed into the coordinates, giving the classical GS Equation in a remapped coordinate system. The new GS coordinates are defined by the gas-pressure scale height, meaning that magnetic fields in a prespecified atmosphere must be spatially distorted. Horizontal flux tubes exhibit substantial radial deformation in a solar corona of given constant temperature (Zweibel & Hundhausen, 1982; Low, 1992). Depending upon their size compared to the gas-pressure scale height, flux tubes are either compressed or expanded in the gravitational direction, and approximately undistorted only in a specific atmosphere.

In §3, we examine equilibrium radial profiles of temperature and flux-tube diameter using an approximate solution to the equilibrium equations. The profiles reproduce the salient features of the solar atmosphere: the rapid expansion of flux tubes in the photosphere where the atmospheric gas pressure is dominant, a transition region of reasonable thickness located just above the height where the gas and magnetic energy densities are equal, and a corona of correct base temperature for the sun’s main magnetic spherical harmonic. Steady flows do not alter the coupling, but may produce a Bernoulli pressure, which modifies the gas pressure, and leads to possible accelerated steady wind solutions.

Although the dynamics of the system can be quite complicated, the equilibrium state characterizes the average in many types of MHD systems, e.g. ‘quasi-steady’ (Low, 1980). Hydrodynamics tend to maintain the MHS atmosphere, as we discuss in §4.

2. MHS equilibria with gravity

The equations for static equilibrium in a gravitational field are the MHS equation and Gauss' Law

$$\nabla p + \frac{p}{h} \nabla r = \frac{1}{4\pi} (\nabla \times \mathbf{B}) \times \mathbf{B}, \quad (3)$$

$$\nabla \cdot \mathbf{B} = 0. \quad (4)$$

The atmospheric contribution to the pressure scale height is directly related to the temperature for a perfect gas, $h \equiv p/(\rho g(r)) = kT/(\bar{m}g(r))$. The variables have their usual meanings: \mathbf{B} is the magnetic field vector in Gaussian units, p the gas pressure, ρ the density, T the temperature, \bar{m} the mean particle mass, k Boltzman's constant, c the speed of light (used below); $g(r) = GM_{\odot}/r^2$ is the gravitational acceleration, with G the universal gravitational constant and M_{\odot} the stellar mass. The coordinate r measures the distance from the system or stellar center, and the formal notation ∇r is adopted for algebraic convenience to denote the radially directed unit vector.

The set of four vector-element equations (3) and (4) contain five unknowns, p , h , and the three vector element of \mathbf{B} . However, the solution space for \mathbf{B} is more restrictive than would be obtained with linear relations, as we discuss in this section and elaborate in Appendix A.

The gravitational term in equation (3) compared to the pressure gradient is of order d/h , where d is a characteristic flux-tube thickness; for the main power in threads in the solar corona $d/h < 10^{-3}$. In the vicinity of non-force-free fields gas-pressure changes must be mainly magnetically determined, and only far away can the gravitational gradient be significant. Where the Lorentz term is negligible, the gas pressure is hydrostatic and defined by a single radial temperature profile. Since the gravitational term is small, the classical equilibrium solutions without gravity described in Appendices A and B are applicable, and equations (1) and (2) valid in every local, but with the allowance that quantities may vary slowly spatially. Thus we obtain coupled atmospheric and magnetic height variations, at least if certain types of flux tubes are present as described in the introduction.

Conditions along field lines are represented by a parallel-field equation

$$\mathbf{B} \cdot \left(\nabla p + \frac{p}{h} \nabla r \right) = 0, \quad (5)$$

which is the projected component of the MHS equation (3) along \mathbf{B} . The relation says that gas pressure changes along field lines must be hydrostatic, which can be seen by introducing the integrating factor ϕ into the gas pressure

$$p = \phi \hat{p}, \quad (6)$$

for an unrestricted function \hat{p} . Upon substitution

$$\mathbf{B} \cdot \left(\phi \nabla \hat{p} + \hat{p} \left(\nabla \phi + \frac{\phi}{h} \nabla r \right) \right) = 0, \quad (7)$$

so taking for the integrating factor

$$\nabla \ln \phi = -\frac{1}{h} \nabla r, \quad (8)$$

we obtain $\mathbf{B} \cdot \nabla \hat{p} = 0$, or \hat{p} constant along field lines. The only solutions to equation (8) are the 1D $\phi = \phi(r)$ and $h = h(r)$ or $T = T(r)$, represented in the hydrostatic relation

$$\frac{\partial \ln \phi(r)}{\partial r} = -\frac{1}{h(r)}, \quad (9)$$

which can be integrated to give

$$\phi(r) = \exp \left(- \int_{r_{\odot}}^r \frac{dr}{h(r)} \right), \quad (10)$$

where r_{\odot} denotes an arbitrary base height for the radial variations. Thus pressure variations along arbitrarily directed field lines follow the 1D hydrostatic scale-height function $\phi(r)$ from a constant base pressure \hat{p} ; 3D effects are possible because the base pressure \hat{p} and the scale-height function $\phi(r)$ or temperature profile $T(r)$ can vary from field line to field line. One scale-height function $\phi(r)$ with temperature profile $T(r)$ applies throughout force-free regions and in isolated non-force-free flux tubes in thermal balance with their local surroundings.

Substituting equation (6) into the MHS equation (3) and using equation (8) gives the cross-field equation

$$\phi(r) \nabla \hat{p} = \frac{1}{4\pi} (\nabla \times \mathbf{B}) \times \mathbf{B}, \quad (11)$$

for \hat{p} allowed to vary from field line to field line. We adopt the single scale-height function $\phi(r)$, assuming for our argument that one temperature profile applies throughout. At a base height r_{\odot} , $\phi(r_{\odot}) = 1$, and the cross-field equation (11) resembles the classical MHS equation (A.1) without gravity. Since the base height r_{\odot} is arbitrary, it is again evident that the classical equilibrium solutions must be applicable in every local.

Since the base pressure \hat{p} is constant along field lines, the variation in the scale-height function $\phi(r)$ on the left side of equation (11) must be reproduced on the right side in the Lorentz term, and so in \mathbf{B}^2 too. Thus \mathbf{B} must vary like $\phi(r)^{1/2}$ along field lines in non-force-free fields within d/h , which is the order of the derivatives of the scale-height function. Formally we can absorb $\phi(r)$ into the magnetic field on the right side by decomposing \mathbf{B} into the general product

$$\mathbf{B} = \phi_B(r) \hat{\mathbf{B}} = \phi_B(r)^{1/2} \hat{\mathbf{B}} = \phi(r)^{1/2} \zeta(r) \hat{\mathbf{B}}. \quad (12)$$

A 1D magnetic scale-height function $\phi_B(r)$ is sufficient to cancel $\phi(r)$; we introduce the residual radial multiplier $\zeta(r)$ to allow differing scale-height functions, leaving $\hat{\mathbf{B}}$ an unrestricted vector function. Substituting back into equations (11) and (4) eliminates $\phi(r)$ and gives

$$\nabla \hat{p} = \frac{1}{4\pi} \left(\left(\nabla - \frac{\nabla r}{2h(r)} \right) \times \zeta(r) \hat{\mathbf{B}} \right) \times \zeta(r) \hat{\mathbf{B}}, \quad (13)$$

$$\nabla \cdot \zeta(r) \hat{\mathbf{B}} = \frac{\nabla r}{2h(r)} \cdot \zeta(r) \hat{\mathbf{B}}. \quad (14)$$

The equations can be solved by substituting perturbative expansions in powers of the small quantity $d/h(r)$, $\hat{p} = \sum_n \hat{p}_n (d/h(r))^n$ and $\hat{\mathbf{B}} = \sum_n \hat{\mathbf{B}}_n (d/h(r))^n$ for $n \geq 0$ with d a constant characteristic flux-tube thickness. The expansions

separate according to powers of $(d/h(r))^n$, giving the most-significant order-zero equations

$$\nabla \hat{p}_0 = \frac{1}{4\pi} (\nabla \times \zeta(r) \hat{\mathbf{B}}_0) \times \zeta(r) \hat{\mathbf{B}}_0, \quad (15)$$

$$\nabla \cdot \zeta(r) \hat{\mathbf{B}}_0 = 0. \quad (16)$$

Equations (15) and (16) in \hat{p}_0 and $\zeta(r) \hat{\mathbf{B}}_0$ are equivalent to the classical plane-parallel MHS equations without gravity, which are discussed in Appendix A. The solutions are the classical equilibria, which exhibit a degenerate direction z in the local coordinate system (x, y, z) taken to be arbitrarily oriented with respect to the radial r . There is no loss in generality in just taking $\zeta(r) = 1$ and $\phi_{B2}(r) = \phi(r)$ in equation (12) leaving $\hat{\mathbf{B}}_0$ the unperturbed solution from equation (A.5) and constant in z . If $z \not\perp r$ the solutions for \mathbf{B} exhibit a variation along the field direction that goes like $\phi(r)^{1/2}$. In the case considered by Dungey (1953) with $z \perp r$, distortion effects are introduced perpendicular to main magnetic field direction like described in the introduction. Thus $h_B(r) = 2h(r)$ at every r , where the magnetic scale height is defined in the usual way, $h_B(r) = -[\partial \ln \phi_B(r) / \partial r]^{-1}$. The scale heights are coupled to most-significant order in the perturbing gravitational field in all non-force-free MHS equilibria containing thin flux tubes in thermal balance with their local surroundings.

The additional perturbative terms, which are developed in Appendix C, give base functions \hat{p} and $\hat{\mathbf{B}}$ that may include small 3D effects introduced with the two small terms $\nabla r / (2h(r))$ in equations (13) and (14). The term on the right side of equation (14) is needed since a slow radial decrease in $|\mathbf{B}|$ cannot occur without a divergence of field lines; the term represents a compensating creation of flux in $\hat{\mathbf{B}}(r)$ with r . The small term added to the curl in the Lorentz force in equation (13) originates with the rescaling of the magnetic field vector in r also. It corresponds to a small residual pseudo-force directed between $\hat{\mathbf{B}}$ and the outward radial ∇r . Such a term arises with a progressive left-handed twist of field lines at the rate of 1 radian in every magnetic scale height $2h(r)$. In MHS equilibria with gravity, the amplitude, the divergence, and the curl of \mathbf{B} all vary on the large scale $2h(r)$.

In principle, a single thin flux tube somewhere in the atmosphere, evacuated or in thermal balance with its surroundings, fixes the equilibrium gas pressure for the entire atmosphere, but all non-force-free fields must be consistent to satisfy mutually the horizontal pressure boundary condition. In reality of course, magnetic fields may exhibit local deviations, and the equilibrium state can really only be viewed as the average in an atmosphere containing many flux tubes.

A flux tube in thermal balance satisfies the condition $p_e(r) \propto \mathbf{B}_e(r)^2$ whether of increased or decreased field strength compared to the local background magnetic field. A flux tube with increased field strength $|\mathbf{B}_i(r)| > |\mathbf{B}_e(r)|$ must exhibit a decreased internal gas pressure in equation (1) $p_i(r) < p_e(r)$, consistent with the extreme dark-thread evacuated case of $p_i(r) = 0$, which requires the minimum surrounding atmosphere for a given relative magnetic field strength. Flux tubes with less field strength than the external magnetic field, $|\mathbf{B}_i(r)| < |\mathbf{B}_e(r)|$, must have an increased gas pressure $p_i(r) > p_e(r)$ consistent with bright threads.

Threads appear to be isolated thin flux tubes aligned with the background magnetic field and embedded in current sheets in a bimodal amplitude distribution, consistent with the natural equilibrium form discussed in Appendix B. The temperature of bright threads was indeed found to be the same as the external surroundings within observational uncertainties (NK96). The solar EUV coronal temperature for unresolved quiet and active regions is relatively uniform, $1.5 - 2.1 \times 10^6$ K (Withbroe, 1975), and a narrow temperature range around 2×10^6 K is found for a broad range of sizes and densities of X-ray loops for all but prominence flare loops (Davis et al., 1975; Vaiana et al., 1976; Rosner et al., 1978). Large-area coronal temperatures derived from the solar white-light scale height and forbidden line ratios give temperatures somewhat lower than the EUV and X-ray temperatures, in the range of $1 - 2 \times 10^6$ K at $r = 1.15r_\odot$ (Guhathakurta et al., 1992).

A slightly heated (or cooled) flux tube has an increased (or decreased) internal pressure $p_i(r)$ and thereby must affect a decreased (or increased) internal field strength $|\mathbf{B}_i(r)|$ or an increased (or decreased) external pressure $p_e(r)$ to satisfy the equilibrium equation (1). Small changes in internal field strength might be accommodated by changes in the flux-tube size as a state of local stress in the large-scale magnetic field, and changes in the surrounding ambient pressure $p_e(r)$ might be modified by compensating external dynamics like we describe in §4. Hot flux tubes will naturally cool to the temperature of their immediate surroundings, bringing them back to the normal MHS equilibrium condition. A relatively cool nonevacuated flux tube with excess field strength tends to evacuation with height as a different equilibrium condition, and so might just persist out of equilibrium within about one internal scale height of its base.

Continuous 3D non-force-free equilibrium solutions are claimed (Low, 1985, 1991), but these allow an arbitrary hydrostatic 1D gas pressure independent of the magnetic field (see the use of $p_0(r)$ and discussion around equation (24) of Low 1991, in §III in Bogdan & Low 1986, or §4 in Neukirch 1997). In the general force balance, that is the cross-field equation (11) with $\phi(r)$ allowed to vary from field line to field line, the pressure and magnetic variations cannot be separated except in force-free regions unconstrained by a horizontal pressure boundary condition, e. g. lacking thin non-force-free flux tubes.

We have confined our study here to the static solutions, but it is straightforward to broaden consideration to include certain types of steady flows. Steady uniform flows along field lines add a flow pressure to the parallel-field equation (5), which leads to a modified hydro-steady relation in equations (9) and (10), but the same cross-field equation (11) results. Thus we obtain a gas pressure containing atmospheric and wind components coupled to the large-scale magnetic field outside flux tubes. Flux-tube flows modify the coupling, and may compensate the equilibrium balance around flux tubes in regions where magnetic radial variations deviate from the norm.

Uniform radial wind flows in a force-free or parallel-field hydro-steady relation exhibit a quite different run of temperature for a given radial run of gas pressure than those derived based upon the hydrostatic equation (9). For a given scale-

height function $\phi(r)$, as might be defined by the magnetic field in a magnetically dominated regime like a lower stellar corona, the atmospheric part of the scale height $h(r)$ and corresponding temperature $kT(r) = \bar{m}g(r)h(r)$ are always larger with a steady flow than without (Parker, 1960).

3. Model atmospheres

The derivation of an explicit static equilibrium solution is a formidable task, because such an analysis must consider the specific form that distorted magnetic fields take in the presence of a gas. However an approximate coupled scale-height function can be written

$$\tilde{\phi}(r) = \phi_a(r) + \frac{1}{\beta_\odot} \phi_{B2}(r), \quad (17)$$

where $\phi_a(r)$ and $\phi_{B2}(r)$ are nominal separate gas and magnetic pressure solutions to the MHS equations (3) and (4) normalized at a base height r_\odot ; the coefficient $1/\beta_\odot$ defines the relative magnetic-field strength. The approximate coupled scale-height function $\tilde{\phi}(r)$ is proportional to the total pressure $p + \mathbf{B}^2/(8\pi)$ of the nominal separate solutions. The gradient of the total pressure approximates the gas-pressure gradient minus the Lorentz term in the MHS equilibrium equation (3) reflecting the local balance in equation (1), as discussed at the end of Appendix B. The coupled scale-height function $\tilde{\phi}(r)$ thus gives a correct MHS solution where one pressure component is dominant, $p \gg \mathbf{B}^2/(8\pi)$ or $\mathbf{B}^2/(8\pi) \gg p$.

At a base height r_\odot , which we take as the stellar photospheric surface, only a small fraction of the area is occupied by magnetic fields, $\beta_\odot \gg 1$ and $\tilde{\phi}(r) \simeq \phi_a(r)$. There the gas pressure is dominant and must follow its nominal atmospheric form, not being much affected by the magnetic field, whereas the magnetic field lines must be highly distorted. Correspondingly the atmospheric-pressure scale-height function $\phi_a(r)$ represents a nominal hydrostatic solution for the gas alone, i.e. equation (9) with a temperature found by using a transfer equation that includes all of the usual energy input and loss mechanisms.

The atmospheric contribution $\phi_a(r)$ characteristically falls off much more rapidly than the magnetic pressure $\phi_{B2}(r)$, so around some transition height r_t where $\phi_a(r_t) = \phi_{B2}(r_t)/\beta_\odot$, $\tilde{\phi}(r)$ changes from $\phi_a(r)$ to $\phi_{B2}(r)/\beta_\odot$ over about one gas-pressure scale height. Above r_t the magnetic field is dominant, $\tilde{\phi}(r) \simeq \phi_{B2}(r)/\beta_\odot$, and the field must follow a nominal form irrespective of the gas pressure. There the gas pressure profile may be very distorted from the nominal, representing an added atmospheric heating produced by MHS restoring flows as we discuss in §4.

Both the magnetic and gas pressure variations must be distorted from their nominal separate forms around the intermediate transition height r_t . Preserving the total pressure $p + \mathbf{B}^2/(8\pi)$ gives an approximate flux-conserving extrapolation below the magnetically dominated corona and an ostensible gas-pressure extrapolation above the photosphere and chromosphere. The total relative pressure around the intermediate transition height goes from $A_T(\phi_a(r) + \phi_{B2}(r)/\beta_\odot)$ for a nominal superposition of independent gas and magnetic pressures $\phi_a(r)$ and $\phi_{B2}(r)/\beta_\odot$

with A_T the total surface area, to $(A_T - A_e)\tilde{\phi}(r) + A_B\tilde{\phi}(r)$ for the coupled pressure $\tilde{\phi}(r)$ with A_e the evacuated area and A_B the magnetically filled area. The two pressure totals are equal in general only with $\tilde{\phi}(r)$ from equation (17) and when the field-filling regions are evacuated with $A_B = A_e$. Anyway the choice of coupled scale-height function is not too critical for our demonstration, as smooth switching functions with correct asymptotic behavior in the photosphere and corona exhibit similar temperature profiles even around the transition height.

For demonstration purposes, we take $\phi_a(r)$ for a polytrope atmosphere as derived in Appendix D

$$\phi_a(r) = \left(1 - \frac{\Gamma - 1}{\Gamma} \frac{r_\odot}{h_\odot} \left(1 - \frac{r_\odot}{r}\right)\right)^{\frac{\Gamma}{\Gamma-1}}, \quad (18)$$

where $h_\odot \equiv h(r_\odot) = kT_\odot/(\bar{m}g_\odot)$ denotes the surface scale height and Γ the ratio of specific heats or polytrope adiabat.

A nominal scale-height function $\phi_{B2}(r)$ is defined for a single-spherical-harmonic potential magnetic field. The potential magnetic form seems to be consistent with what is observed in the lower solar corona for $r < 1.6r_\odot$ (Altschuler & Newkirk, 1969; Schatten et al., 1969). The potential magnetic field vector is the gradient of a sum of scalar spherical-harmonic component functions, each of which is the separable product of a 2D surface function and radial multiplier $1/r^{\ell+1}$. The resulting magnetic field in each spherical harmonic goes like $1/r^{\ell+2}$ in all its vector elements; a monopole $\ell = 0$ exhibits a $1/r^2$ radial falloff, a dipole field $\ell = 1$, a $1/r^3$ falloff, etc. For a single spherical harmonic ℓ , the magnetic energy density falls off like

$$\phi_{B2}(r) = \left(\frac{r_\odot}{r}\right)^{2\ell+4}. \quad (19)$$

With a superposition of spherical harmonics, a nonuniform radial dependence can occur, and a representative global-average spherical harmonic ℓ might be obtained by appropriately weighting flux-tube locations.

The temperature is written from the hydrostatic equation (9)

$$kT(r) = \bar{m}g(r)h(r) = -\bar{m}g(r) \left(\frac{1}{\phi(r)} \frac{\partial \phi(r)}{\partial r}\right)^{-1}. \quad (20)$$

Taking $\phi(r)$ to be the approximate $\tilde{\phi}(r)$ from equation (17) with $\phi_a(r)$ from equation (18) and $\phi_{B2}(r)$ from equation (19), we obtain an explicit formula for $T(r)$. In the corona $\phi(r) \simeq \phi_{B2}(r)/\beta_\odot$, and the formula exhibits the limiting scale height

$$h_{\text{cor}}(r) = \frac{r}{2\ell + 4}, \quad (21)$$

and temperature

$$kT_{\text{cor}}(r) = \frac{GM_\odot \bar{m}}{(2\ell + 4)r} = \frac{\bar{m}g(r)r}{2\ell + 4}. \quad (22)$$

The limiting base coronal temperature $T_{\text{cor}}(r_\odot)$ is defined entirely by the stellar surface gravity g_\odot , radius r_\odot , mean particle mass \bar{m} , and main magnetic spherical harmonic ℓ . For a toroidal field $\ell = 2$, the scale height at the stellar surface is $h_{\text{cor}}(r_\odot) = r_\odot/8$, which gives a solar base coronal temperature of $T_{\text{cor}}(r_\odot) = 1.73 \times 10^6$ K (using $\bar{m} = 0.6m_p$ for m_p the proton

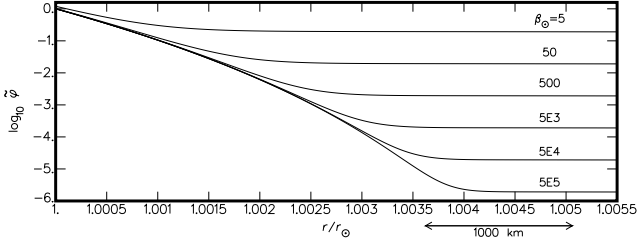


Fig. 2. Log of scale-height function $\log_{10} \tilde{\phi}(r)$ for a solar polytrope atmosphere with $\Gamma = 1.1$ and a potential magnetic field $\ell = 2.33$ for different inverse base fields β_∞ .

mass, $\bar{m} = 1 \times 10^{-24}$ g, $r_\infty = 6.96 \times 10^{10}$ cm, $g_\infty = 2.75 \times 10^4$ cm s $^{-2}$, and $k = 1.38 \times 10^{-16}$ ergs K $^{-1}$). With the solar base coronal temperature of $T_{\text{cor}}(r_\infty) = 1.6 \times 10^6$ K, we obtain the spherical harmonic $\ell = 2.33$.

Figure 2 shows some example scale-height functions $\tilde{\phi}(r)$ from equations (17 – 19) in the lowest part of the solar atmosphere around the transition height r_t . Scale-height functions with the polytrope adiabat $\Gamma = 1.1$ and spherical harmonic $\ell = 2.33$ are plotted for different inverse base-field strengths β_∞ , using the solar parameters and surface photospheric temperature $T_\infty = 6820$ K from the VAL model atmospheres (Vernazza et al., 1981), which defines the surface scale height $h_\infty = kT_\infty/(\bar{m}g_\infty)$ for $\phi_a(r)$ in equation (18). As all of the curves are based on the same Γ , they coincide until the transition height r_t for the model is reached, and then switch rapidly to the nominal magnetic $\phi_{B2}(r)$, which appears to be relatively flat on the log scale.

The radial expansion of a flux tube is another way to visualize the field strength decrease in the atmosphere and the properties of the coupled scale-height function. For conservation of the total flux through the cross-sectional area of a flux tube $\pi(d/2)^2 |\mathbf{B}|$, the flux-tube diameter $d(r)$ must increase with radial distance r , $d(r) \propto |\mathbf{B}|^{-1/2} \propto \phi(r)^{-1/4}$. Figure 3 portrays the relative flux-tube diameter as a function of height $d(r)/d_\infty$ for different solar atmospheric models denoted by Γ and β_∞ .

For a given polytrope adiabat Γ , all flux tubes exhibit approximately the same relative shape up to a height that depends upon β_∞ , where the field lines straighten up. Stronger fields exist with a lower transition height and exhibit less overall relative expansion before straightening up. The canopy depends upon the surface distribution of the fields, but strong fields might give the appearance of a lower canopy height too consistent with the observations of sunspots (Giovanelli & Jones, 1982). The straightening height is somewhat below the location of the fastest temperature change due to the differing dependencies: The field strength, which goes like $\phi(r)^{1/2}$, straightens up from the atmospherically determined form at r_t , but the most rapid temperature change occurs significantly higher where the slope of the scale-height function flattens out, as $T(r) \propto -(\partial \ln \phi(r)/\partial r)^{-1}$.

Figure 4 illustrates the temperature variation in the lower solar atmosphere using equation (20) with $T_\infty = 6820$ K from the VAL atmospheres. The upper panel shows the model atmospheres with $\ell = 2.33$ and $\beta_\infty = 5000$ for different polytrope adiabats Γ , and the lower panel the model atmospheres with

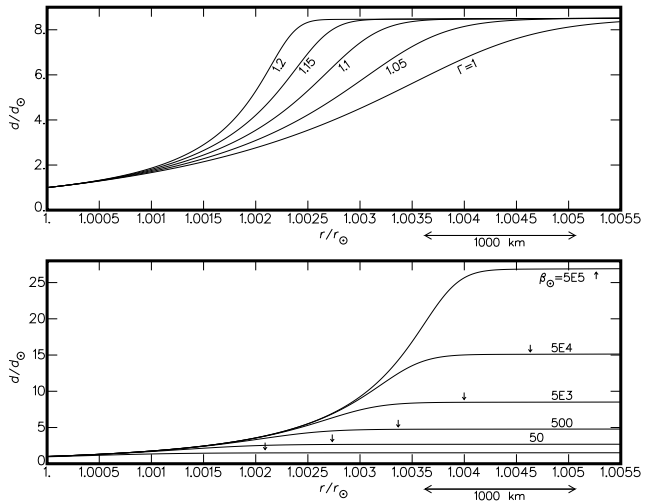


Fig. 3. Relative flux-tube diameter $d(r)/d_\infty$ in lower solar atmosphere with $\ell = 2.33$ and $\beta_\infty = 5000$ for different polytrope adiabats Γ (*upper panel*), and with $\ell = 2.33$ and $\Gamma = 1.1$ for different inverse base fields $\beta_\infty = 5, 50, \dots 5.E5$ (*lower panel*). The arrow on each curve locates the most rapid temperature change for the model.

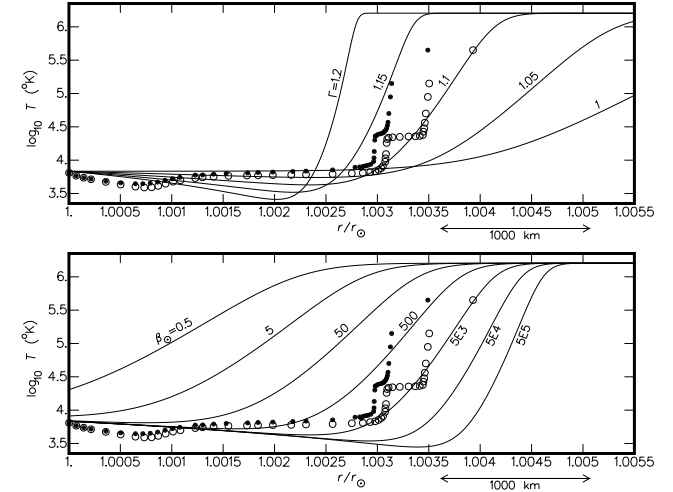


Fig. 4. Lower solar atmosphere $\log_{10} T(r)$ with $\ell = 2.33$ and $\beta_\infty = 5000$ for different polytrope adiabats Γ (*upper panel*), and with $\ell = 2.33$ and $\Gamma = 1.1$ for different photospheric β_∞ (*lower panel*), shown with the solar VAL A (open circles) and F (filled circles) atmospheres.

$\ell = 2.33$ and $\Gamma = 1.1$ for different inverse base fields β_∞ . The VAL A and F model temperatures are shown for relatively cool inner network and hot network bright points, respectively.

In the solar photosphere, the nominal atmospheric polytrope follows the VAL temperature roughly, giving the best tradeoff between photospheric and chromospheric temperatures with $\Gamma \approx 1.1$. Of course the features of a real solar atmosphere can never be well approximated by a polytrope. The shape of the temperature function through the chromosphere and transition height, where the scale-height function $\tilde{\phi}(r)$ goes from $\phi_a(r)$ to $\phi_{B2}(r)/\beta_\infty$, depends upon Γ and β_∞ but not on

ℓ , which separately determines the base coronal temperature. Temperature profiles with $\beta_\odot \simeq 5000$ and $\simeq 1000$ give best agreement around the transition height with the VAL A and F atmospheres, respectively, averaging approximately through the Ly α plateau.

For flux-tube evacuation in the photosphere $B(r_\odot)^2 = 8\pi p(r_\odot)$, and we obtain a maximum field strength of $|B(r_\odot)| = 1715$ G using $p(r_\odot) = 1.17 \times 10^5$ dynes cm $^{-2}$ from the VAL solar models. MHS atmospheres exhibit a general arbitrariness in the base gas pressure, which is contained in the constant β_\odot . Strictly the coefficient $1/\beta_\odot$ represents the coronal base gas or non-force-free magnetic pressure extrapolated back to r_\odot . The extrapolated coronal base pressure can be no larger than the average surface magnetic pressure, but their relationship may be influenced by the detailed field geometry and specific magnetic evolutionary history. Thus the relative area covered by magnetic fields at r_\odot must be at least $1/\beta_\odot^{1/2}$, or $1/71$ for $\beta_\odot = 5000$ and $1/32$ for $\beta_\odot = 1000$, which corresponds to a minimum base coronal field strength of $|B_{\text{cor}}| = 24$ G for $\beta_\odot = 5000$ and $|B_{\text{cor}}| = 54$ G for $\beta_\odot = 1000$, not out of range of solar observations (Lin et al., 2000). A lower transition region occurs where the photospheric flux-tube area coverage and coronal magnetic field strength are larger near active regions, consistent with the known tendency.

The solar atmospheric model of Fontenla et al. (1990), which includes particle diffusion and conduction effects, lacks the Ly α plateau and exhibits a much more abrupt transition region than what we obtain. While radiative, diffusive, and conductive losses must be largely balanced by MHS restoring flows in the corona, as we discuss in §4, loss mechanisms can influence the detailed shape of transition-region profiles. Real radiative models coupled to more general magnetohydro-steady equilibrium solutions need to be developed, but such work may be complicated by the intrinsic limitations and uncertainties in atmospheric modeling, especially associated with inhomogeneous magnetic structure (Ayres, 1981; Carlsson & Stein, 1995). It is possible that general methods based upon transition-region emissivity profiles, which have been used to determine the nonradiative atmospheric heating contribution, might be able to distinguish coronal heating by MHS restoring flows from other heating mechanisms (Craig & Brown, 1976; Anderson et al., 1996).

Figure 5 illustrates the solar atmospheric temperature function $T(r)$ for various values of ℓ with the coronal temperatures inferred from the white-light-intensity radial gradient taken from eclipse photographs (Newkirk et al., 1970) and inferred from FeXIV 5303Å line-width measurements (Jarrett & von Klüber, 1958). The limited resolution in r in the figure hides the transition region near r_\odot . The coronal model for the spherical harmonic $\ell = 1$ seems to give the best overall agreement with the measured radial profiles, but $\ell \simeq 2.3$ better matches the base coronal temperature. However all of the model curves show a more rapid falloff than the measured temperature profiles. Models containing an outward wind should give systematically higher temperatures with height in the corona.

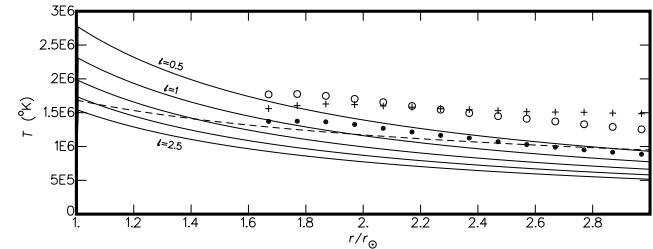


Fig. 5. Static solar corona $T(r)$ for $\ell = .5, 1, 1.5, 2$, and 2.5 (from top to bottom) shown with temperature from white-light intensity in the quiet equator (filled circles), in SW (crosses), and in SE (open circles) streamers (Newkirk et al., 1970), and from line-width measurements (dashed line) (Jarrett & von Klüber, 1958).

4. MHS restoring flows

Under usual conditions, e.g. quasi-steady, the large-scale and long-term system average is represented by the equilibrium state. In the quasi-steady approximation, the system evolution can be described by a sequence of nearby equilibria. The quasi-steady approximation is shown to be applicable when magnetic adjustments are fast compared to evolutionary processes and the magnetic field is dominant over the gas, as in the solar corona (Low, 1977).

Certain dynamical scenarios naturally produce the MHS equilibrium atmosphere. Hydro-steady equilibria are always self-restoring. In the absence of sufficient external gas or flow pressure, a time-dependent outward gas acceleration arises outside and along rigidly held non-force-free flux tubes in the overall MHD balance. The pressure perturbation that drives the flow propagates away from its source at the sound speed in all directions, so as long as the timescale for evolutionary change is relatively long, the MHS equilibrium atmosphere must be the global mean. Flows in a fixed magnetic field act generally to reestablish the equilibrium atmosphere, heating the gas compressively, as described in Appendix E.

Eventually energy losses must overcome MHS restoring flows and cool the atmosphere, reducing the coupled pressure scale height, geometrically stressing the magnetic field, which contributes to magnetic instability. The magnetic field can be perturbed in other ways too, e.g. by new flux coming up from the convection zone below or by photospheric twisting and flux-tube motions. Magnetic evolution is complicated since unstable equilibria are generally possible, that is perturbations that *reduce* the overall energy of the system. Also local deviations may persist within field allowances before equilibria can be resolved. However if the new magnetic equilibrium after fast reconnection is mostly force-free containing thin non-force-free flux tubes, outflows again must reestablish the equilibrium gas-pressure profile of a depleted cool atmosphere, as discussed too in Appendix E.

Other sources of heating may contribute significantly to the overall MHS requirement, adding stability to the large-scale magnetic field and longevity to the evolutionary process. Heat-flux scaling relations in loops and homogeneous regions allow the total coronal energy requirement to be estimated

(Rosner et al., 1978; Hearn & Kuin, 1981; Hammer, 1982). If sufficient magnetic energy is not available from evolutionary processes to offset losses, then pure force-free cool equilibria may be the only possibility. The importance of MHS atmospheres in more marginal non-quasi-steady physical conditions and for other problems in physics and astrophysics needs to be considered, but discussion lies beyond the scope of this paper.

Other heating sources may lead to nonuniform temperatures as well. Localized heating may produce inhomogeneous temperatures in flux tubes (Vaiana & Rosner, 1978). Heated flux tubes must exhibit field-line perturbations that stress the large-scale magnetic field and tend to produce outflows in the surroundings at least on the average, which heat the ambient atmosphere above the normal equilibrium temperature. Such processes can have a relatively large-scale effect since they produce an ambient hydrostatic imbalance, which propagates away much faster than thermal diffusion effects. Post-reconnection hydrodynamic heating acting throughout the coronal volume overcomes the often-cited difficulty that reconnection events are so spatially localized and short-lived that only a larger event rate than what is directly inferred from observations could account for coronal heating (Heyvaerts & Priest, 1984; Hudson, 1991).

Thus MHD processes in general conditions tend to produce refilling outflows, a ‘magnetic suction’, which might be evidenced with the large-scale flows seen in the vicinity of coronal voids (Wagner et al., 1983), or may be responsible for the supergranular-scale chromospheric upward velocities interpreted from solar post-flare spectral-line blue shifts (Schmieder et al., 1987; Cauzzi et al., 1996), or appear as spicule eruptions in the chromosphere. The upward mass flux produced by solar spicule events is about 100 times the total wind mass flux, but represents only a small fraction of the total wind energy flux (Pneuman & Kopp, 1978).

The remarkable feature of an MHS corona is that the temperature is essentially a geometric parameter defined by the stellar surface gravity g_\odot , radius r_\odot , mean particle mass \bar{m} , and magnetic spherical harmonic ℓ

$$kT_{\text{cor}}(r_\odot) = \frac{\bar{m}g_\odot r_\odot}{2\ell + 4}. \quad (23)$$

The observed average solar base coronal temperature of 1.6×10^6 K corresponds to a spherical harmonic of $\ell = 2.33$ consistent with the large-scale solar magnetic field, which exhibits substantial power in the toroidal $\ell = 2$ and spherical harmonics $\ell = 3$ or 4 as evidenced by the presence of active longitudes. With a general mixture of spherical harmonics, discrepant horizontal gas-pressure boundary conditions at flux tubes can arise, and a nonuniform large-scale surface temperature distribution is possible as a deviation from the pure MHS equilibrium state.

Our formula for the average base coronal temperature, equation (23), has been suggested already in the hypothesis of a ‘geometric boundary condition’, relevant for different kinds of heating models that exhibit a base pressure scale height proportional to the stellar radius (Menzel, 1968; Scudder, 1992). The formula appears to give accurate coronal temperatures for a range of stellar types (Williams & Mullan, 1996).

Acknowledgements. The author is grateful to many for useful discussion during the course of this work, especially to Eric Priest and Ray Smartt for their careful reviews of the manuscript, and to the referee for many insightful remarks and helpful suggestions.

Appendix A: Local MHS equilibria

There are well-known solutions to the classical static problem describing a gas existing in conjunction with elongated magnetic fields without a perturbing gravitational field (Parker, 1979, Chapter 6). It is helpful to revisit the classical problem here in a general way. The classical MHS equilibrium equations without gravity are the static equilibrium equation

$$\nabla p = \frac{1}{4\pi}(\nabla \times \mathbf{B}) \times \mathbf{B}, \quad (A.1)$$

and Gauss’ Law, equation (4).

Plane-parallel solutions can be developed based upon the general Cartesian vector function

$$\mathbf{B} = \left(\frac{\partial a(\mathbf{x})}{\partial y}, -\frac{\partial a(\mathbf{x})}{\partial x} - \frac{\partial b(\mathbf{x})}{\partial z}, \frac{\partial b(\mathbf{x})}{\partial y} \right). \quad (A.2)$$

The x and z vector elements of \mathbf{B} , $\partial a/\partial y$ and $\partial b/\partial y$, are taken to be arbitrary functions, and the y element is written so that Gauss’ Law is always satisfied. It is convenient to use derivative forms in the vector elements to avoid complicating integrals in the expression.

Any solutions to equation (A.1) must satisfy the two conditions $\mathbf{B} \cdot \nabla p = 0$ and $(\nabla \times \mathbf{B}) \cdot \nabla p = 0$, which are written with \mathbf{B} from equation (A.2)

$$C_{xy}a - C_{yz}b = 0, \quad (A.3)$$

$$\left(C_{xz} \frac{\partial}{\partial x} + C_{yz} \frac{\partial}{\partial y} \right) a + \left(C_{xy} \frac{\partial}{\partial y} + C_{xz} \frac{\partial}{\partial z} \right) b = 0, \quad (A.4)$$

using the linear commutation operators $C_{xy} \equiv (\partial p/\partial x)(\partial/\partial y) - (\partial p/\partial y)(\partial/\partial x)$, etc., which contain $p(\mathbf{x})$ as an implicit function.

The two equations (A.3) and (A.4) can be used to write two of the functions in terms of the third, e.g. $a(\mathbf{x})$ and $b(\mathbf{x})$ in terms of $p(\mathbf{x})$. The third relation, equation (A.1) in the vector direction perpendicular to both \mathbf{B} and $\nabla \times \mathbf{B}$, gives a differential relation for the third quantity. The separate vanishing of all of the commutator terms is a reduction that is satisfied with certain general functional dependencies between the variables and leads to a well-known self-consistent form for the third equation, the Grad-Shafranov Equation. Other possibilities are not considered here.

Taking all the commutator terms to vanish in equations (A.3) and (A.4), but without other reduction, gives $a(\mathbf{x})$, $b(\mathbf{x})$, and spatial derivatives of $a(\mathbf{x})$ and $b(\mathbf{x})$ as functions of $p(\mathbf{x})$ alone, which is only possible for certain trivial spatial forms for real functions, so other reductions are required. Taking $\partial/\partial z = 0$ gives a consistent solution defined by the functional dependencies $a = a(p(x, y))$ in equation (A.3) and $\partial b/\partial y = (\partial b/\partial y)(p(x, y))$ in equation (A.4). A similar solution is obtained by taking $\partial/\partial x = 0$. These two solutions or linear combinations are equivalent with rotation of the $x - z$ axes around

y . Taking z as the degenerate direction gives the usual 2D solution, ordinarily written with a as the implicit function

$$\mathbf{B} = \left(\frac{\partial a(x, y)}{\partial y}, -\frac{\partial a(x, y)}{\partial x}, B_z(a(x, y)) \right). \quad (\text{A.5})$$

The degenerate z is a direction of field elongation. The magnetic potential function $a(x, y)$ defines a 2D planform for the solutions, which determines the spatial variations in the longitudinal field element $B_z = B_z(a(x, y))$ and gas pressure $p = p(a(x, y))$ as arbitrary 1D mappings. The magnetic field is everywhere perpendicular to the gradient of $a(x, y)$, since $\mathbf{B} \cdot \nabla a(x, y) = 0$.

It is widely believed that this 2D solution is the only plane-parallel one. Using perturbative expansions, Parker shows that no nearby 3D solutions exist for bounded quantities in an infinite spatial domain (Parker, 1979, Section 14.2). However 3D variations do arise as large-scale deviations from plane parallel (Arendt & Schindler, 1988). In the common shorthand, ‘2.5D’ solutions refer to perturbed solutions in the problem with gravity, which admit large-scale variations in the degenerate direction of the magnetic field.

Appendix B: Properties of local MHS equilibria

Substituting \mathbf{B} from equation (A.5) into equation (A.1) gives the governing equation for the implicit magnetic potential function $a(x, y)$ for the static equilibrium problem without gravity

$$\left(\nabla^2 a + \frac{d}{da} \left(4\pi p(a) + \frac{B_z(a)^2}{2} \right) \right) \nabla a = 0. \quad (\text{B.1})$$

Where $\nabla a \neq 0$, the potential function must satisfy the Grad-Shafranov (GS) Equation, written

$$\nabla^2 a(x, y) = -P'(a(x, y)), \quad (\text{B.2})$$

defining the total pressure $P(a) = 4\pi p(a) + B_z(a)^2/2$, where $P'(a) = dP(a)/da$.

The total pressure $P(a)$ and its component functions $p(a)$ and $B_z(a)$ are all one dimensional and nonlinear but must all be well-defined everywhere in the solution domain consistent with their forms at the boundaries. Strictly, disagreeing z boundary conditions are inconsistent with the z independence of the solutions; differences might produce small deviations in the solutions like twist or divergence or be a source of dynamical instability. It is popular to restrict consideration to entirely force-free solutions with $p'(a) = 0$; the restriction does not change the nature of the basic GS Equation (B.2) for $a(x, y)$ but requires the specific current density $\mathbf{J} = (c/(4\pi))B_z'(a)\mathbf{B}$ for an arbitrary $B_z(a)$, as is evident by expanding $\mathbf{J} \equiv (c/(4\pi))\nabla \times \mathbf{B}$ using \mathbf{B} from equation (A.5) with $\mathbf{J} \propto \mathbf{B}$.

The magnetic potential function a can be seen to be constant everywhere in the local plane of \mathbf{B} and \mathbf{J} . From equation (A.1), $\mathbf{J} \cdot \nabla p(a) = 0$. Then $\mathbf{J} \cdot \nabla p(a) = (\mathbf{J} \cdot \nabla a) p'(a) = 0$. Thus $\mathbf{J} \cdot \nabla a = 0$ at least when $p'(a) \neq 0$, and when $p'(a) = 0$, $\mathbf{J} \parallel \mathbf{B}$ so $\mathbf{J} \cdot \nabla a = 0$ anyway. We think of a as constant on ribbon-like current sheets with possible embedded flux-tube anomalies along \mathbf{B} , the solution surfaces being more curved along \mathbf{J} as it is defined by the derivatives of \mathbf{B} .

The GS Equation (B.2) has the unusual feature that it contains the 1D filter function $P'(a)$. For the linear case, $P'(a) = k_0^2 a$ with k_0 a constant wavenumber, and the Fourier transform of the GS Equation gives a transform function $\bar{a}(k_x, k_y)$ that is zero everywhere in its 2D wavenumber domain $\mathbf{k} = (k_x, k_y)$ except on a thin annulus at $|\mathbf{k}| = k_0$, where arbitrary complex values Hermitian in $\pm \mathbf{k}$ are allowed. Taking the Fourier transform back gives a potential function $a(x, y)$ that is a spatial distribution of delta-function source points convolved with a common Bessel-function radial kernel times azimuthal factor. Boundary conditions on $a(x, y)$ constrain the azimuthal factor, leading to possible planar solutions defined by all power at one azimuth, or axisymmetric solutions with power uniformly distributed in azimuth, consistent with the visualization of current sheets with embedded cylindrical flux tubes. Physical arguments show that nonlinear kernels are similarly constrained by boundary conditions (Vainshtein & Parker, 1986).

Random spatial distributions of a common GS kernel are nonlinear GS solutions too. We take the potential function $a(x, y)$ to be the convolution of a distribution of sources $D(x, y)$ with a common 2D kernel function $A(x, y)$, $a(x, y) = D(x, y) * A(x, y)$. The distribution is written $D(x, y) = \sum_j c_j \delta(x - x_j, y - y_j)$ counting sources j of varying strength c_j , where $\delta(x, y)$ denotes the 2D delta function. For a spatially incoherent or random distribution D of equal strength sources with all $c_j = 1$, D raised to a power is D alone; for equal amplitude sources with $c_j = \pm 1$, D raised to an odd power is D alone. For an analytic nonlinear driver function $P(a)$, the convolution with an incoherent distribution in D of suitably restricted amplitudes factors out $P'(a) = P'(D * A) = D * P'(A)$, and the GS Equation (B.2) reduces to the same GS Equation but for the common kernel function A in place of a . Dark and bright threads are probably isolated thin flux tubes aligned with the background magnetic field embedded in current sheets suggestive of a bimodal amplitude distribution of a common flux-tube kernel.

Parker (1972) considers MHS equilibria that contain a relatively strong constant background field. Expanding the Lorentz term in equation (A.1) gives an alternate form for the MHS equation

$$\nabla \left(p + \frac{\mathbf{B}^2}{8\pi} \right) = \frac{1}{4\pi} (\mathbf{B} \cdot \nabla) \mathbf{B}, \quad (\text{B.3})$$

or with the superposition $\mathbf{B}(\mathbf{x}) = \mathbf{B}_e + \mathbf{B}_\sim(\mathbf{x})$ for a constant background field \mathbf{B}_e and a spatially varying field $\mathbf{B}_\sim(\mathbf{x})$, we obtain

$$\nabla \left(p + \frac{\mathbf{B}^2}{8\pi} \right) = \frac{1}{4\pi} (\mathbf{B}_e \cdot \nabla) \mathbf{B}_\sim + \frac{1}{4\pi} (\mathbf{B}_\sim \cdot \nabla) \mathbf{B}_e. \quad (\text{B.4})$$

Taking the divergence and applying Gauss's Law $\nabla \cdot \mathbf{B}_\sim = 0$ and using the property that the total pressure $p + \mathbf{B}^2/(8\pi)$ is a bounded quantity in an infinite domain, we obtain

$$(\mathbf{B}_e \cdot \nabla) \mathbf{B}_\sim = 0, \quad (\text{B.5})$$

at least to first order in the small quantity $|\mathbf{B}_\sim|/|\mathbf{B}_e|$. Thus we have

$$\nabla \left(p + \frac{\mathbf{B}^2}{8\pi} \right) \simeq 0. \quad (\text{B.6})$$

to first order in $|\mathbf{B}_\sim|/|\mathbf{B}_e|$. Equation (B.5) proves to be accurate to all orders in the perturbative expansions, and the equilibrium equations (1) and (2) are justified at least in the presence of a relatively strong constant background field, where the internal flux-tube field is defined $\mathbf{B}_i \equiv \mathbf{B}_e + \mathbf{B}_\sim (= \mathbf{B})$. Additional discussion on Parker's perturbative expansion is contained in Appendix C.

The Parker theorem equation (B.5) reflects the special features of the classical equilibria in equation (A.5) in the degenerate direction of the magnetic field z . MHS equilibria only allow certain alignments for the background field. A constant magnetic field can enter into the z vector element $B_z(A)$ without producing other ramifications, whereas an added offset in the x or y elements of \mathbf{B} requires adding a uniformly inclined plane to $a(x, y)$. Such a plane limits the solutions and thus cannot be considered general, and even appears to be precluded by the boundedness of $a(x, y)$: Low-wavenumber components in the Fourier domain needed to represent the added plane are at odds with the Fourier ring solutions for the linear GS equation (B.2) and also contrary to the form of a superposition of spatially compact axisymmetric nonlinear kernels.

Appendix C: Perturbative expansions

The less-significant order $n > 0$ equations in the perturbative series developed from equations (13) and (14) are written for $\zeta(r) = 1$; from the MHS equation (13)

$$\nabla \hat{p}_1 - \frac{1}{4\pi} ((\nabla \times \hat{\mathbf{B}}_0) \times \hat{\mathbf{B}}_1 + (\nabla \times \hat{\mathbf{B}}_1) \times \hat{\mathbf{B}}_0) = \frac{1}{8\pi d} (\nabla r \times \hat{\mathbf{B}}_0) \times \hat{\mathbf{B}}_0, \quad (\text{C.1})$$

or for the general order $n > 0$

$$\nabla \hat{p}_n - \frac{1}{4\pi} \sum_{j=0}^n (\nabla \times \hat{\mathbf{B}}_j) \times \hat{\mathbf{B}}_{n-j} = \frac{1}{8\pi d} \sum_{j=0}^{n-1} (\nabla r \times \hat{\mathbf{B}}_j) \times \hat{\mathbf{B}}_{n-j-1} \left(1 + 2j \frac{\partial h(r)}{\partial r} \right). \quad (\text{C.2})$$

From equation (14)

$$\nabla \cdot \hat{\mathbf{B}}_1 = -\frac{1}{2d} (\nabla r \cdot \hat{\mathbf{B}}_0), \quad (\text{C.3})$$

or in general for $n > 0$

$$\nabla \cdot \hat{\mathbf{B}}_n = -\frac{1}{2d} (\nabla r \cdot \hat{\mathbf{B}}_{n-1}) \left(1 + 2(n-1) \frac{\partial h(r)}{\partial r} \right). \quad (\text{C.4})$$

The equations are linear in the variables \hat{p}_n and $\hat{\mathbf{B}}_n$ based upon order $< n$ variables. The order-zero base functions \hat{p}_0 and $\hat{\mathbf{B}}_0$ are 2D and constant in the degenerate magnetic field direction z ; 3D effects are introduced in order $n > 1$ with general variation in the function $h(r)$ with r not perpendicular to z . For consistency in equations (13) and (14), $\hat{\mathbf{B}}_0 \cdot \nabla \hat{p}_0 = 0$, which is the order-zero component of $\mathbf{B} \cdot \nabla \hat{p} = 0$.

A wide latitude is allowed for choosing perturbative quantities, and as long as they are relatively small most everywhere the standard procedure remains valid. Van Ballegooijen (1985) questions the Parker (1972) choice of perturbative quantity and equation separation procedure, but Van Ballegooijen's assigning of approximate magnitudes to individual factors in his paper to separate his equations is not an algebraic procedure, and his resulting equations have inherent contradictions (Parker,

1987). Parker (1972) does not ascribe a particular functional meaning to his kernel ϵ as he says at the beginning of his §II: "Expand the field \mathbf{b} and pressure p in ascending powers of *some* parameter ϵ , which is of the order of $\epsilon = |\mathbf{b}|/|\mathbf{B}|$ ", where \mathbf{b} is the small spatially varying magnetic field on the uniform background field \mathbf{B} . Our choice for perturbative kernel $d/h(r)$ with d constant leads to a convenient separation of orders.

The perturbative procedure is a functional separation method rooted in the natural independence of the basis functions ϵ^n irrespective of their real amplitudes. If the parameter ϵ is small almost everywhere, the series solutions will be convergent. It may be true as Van Ballegooijen contends that there could be locations where the amplitude of some normally small expansion parameter ϵ actually becomes relatively large. There series expansions are divergent, but such behavior characteristically defines the isolated singularities of ordinary differential equations as discussed in theorems on the Frobenius method for series solutions.

Appendix D: Polytrope atmosphere

A polytrope atmosphere is defined by the pressure relation $p(r) \propto \rho(r)^\Gamma$ for the polytrope adiabat Γ . Thus the 1D polytrope scale height $h(r) = p(r)/(\rho(r)g(r))$ can be written

$$\frac{h(r)}{h_\odot} = \left(\frac{p(r)}{p(r_\odot)} \right)^{\frac{1}{\Gamma-1}} \frac{g_\odot}{g(r)} = \phi(r)^{\frac{1}{\Gamma-1}} \frac{g_\odot}{g(r)}, \quad (\text{D.1})$$

making reference to a base height r_\odot taken usually to be the stellar surface, and introducing the scale-height function $\phi(r)$ for the normalized gas pressure.

Substituting $h(r)$ into the hydrostatic equation (9) defines the scale-height function for a polytrope

$$\phi(r)^{-1/\Gamma} \frac{\partial \phi(r)}{\partial r} = -\frac{g(r)}{g_\odot h_\odot}, \quad (\text{D.2})$$

or

$$\frac{\partial}{\partial r} \phi(r)^{\frac{\Gamma-1}{\Gamma}} = -\frac{\Gamma-1}{\Gamma} \frac{g(r)}{g_\odot h_\odot}. \quad (\text{D.3})$$

The differential equation is easily solved, giving

$$\phi(r) = \left[-\frac{\Gamma-1}{\Gamma} \int \frac{g(r)}{g_\odot h_\odot} dr \right]^{\frac{1}{\Gamma-1}}, \quad (\text{D.4})$$

and with $g(r) = g_\odot (r_\odot/r)^2$, we obtain

$$\phi(r) = \left[1 - \frac{\Gamma-1}{\Gamma} \frac{r_\odot}{h_\odot} \left(1 - \frac{r_\odot}{r} \right) \right]^{\frac{1}{\Gamma-1}}, \quad (\text{D.5})$$

choosing the constant of integration so that $\phi(r_\odot) = 1$. The part of the expression contained in brackets [] represents the radial temperature variation, the thermal lapse rate. The polytrope adiabat Γ ranges from 1 to $5/3$ for an atmosphere ranging from lossy and isothermal to adiabatically stratified. For $\Gamma = 1$, the scale-height function $\phi(r)$ has a limiting pure exponential decay form. For $\Gamma > 1$, the thermal lapse rate and scale-height function have the unphysical feature that they become negative at some height, showing that a polytrope of constant Γ can exist only over a limited range in r . Such behavior is well known in stellar-interior polytrope models and leads to a well-defined top in convection zones.

Appendix E: Hydrodynamics around fixed fields

If the magnetic field is dominant over the gas, and either the field remains stationary, or the magnetic adjustment time is much shorter than the hydrodynamic adjustment time, then the Lorentz term in the MHD equation can be treated as constant in time and the hydrodynamics separate from the magnetodynamics.

Fast magnetic adjustment is a remarkable feature of solar reconnection phenomena. Sporadic crossings of coronal loops in low-energy flare events (Lin et al., 1992) suggest ‘X’-type configurations, and the instability of the ‘X’ configuration is well known to form a new current sheet at near the Alfvén velocity if a nonzero resistivity can be affected in the region (Dungey, 1958; Syrovatskii, 1981); such a resistivity is predicted in some models (Petschek & Thorne, 1967; Priest, 1972). Taking a field strength of $|\mathbf{B}| \simeq 400$ G as representative of chromospheric magnetic fields near neutral lines in solar active regions where flares commonly occur, we obtain an Alfvén speed $c_a = |\mathbf{B}|/(4\pi\rho)^{1/2} \simeq 10^8$ cm s⁻¹ (with $\rho = N\bar{m} = 10^{-12}$ g cm⁻³, using $N = 10^{12}$ cm⁻³ and $\bar{m} = 10^{-24}$ g). The Alfvén speed stays fairly constant into the corona giving a collapse time of $\tau_B = h_B/c_a \simeq 160$ s for the propagation of the instability through a magnetic scale height $h_B = 2h_{\text{cor}} = r_\odot/(\ell + 2) \simeq 1.6 \times 10^{10}$ cm, using a primary magnetic spherical harmonic of $\ell = 2.33$ in equation (21).

The hydrodynamic response to already present or newly formed isolated thin non-force-free flux tubes can be obtained by perturbative analysis of the dynamical equations projected along the magnetic field. Taking the velocity to be aligned with the magnetic field and of lesser order than the mean quantities adds a single time-derivative term to the basic equation (3) and the component along the field written with the continuity equation

$$\rho \frac{\partial u_1}{\partial t} + \frac{\partial p}{\partial z} + \rho g(\nabla z \cdot \nabla r) = 0, \quad (\text{E.1})$$

$$\frac{\partial \rho}{\partial t} + \frac{\partial}{\partial z}(\rho u_1) = 0, \quad (\text{E.2})$$

which are taken with the thermodynamic energy equation $p \propto \rho^\gamma$; z is the direction of the magnetic field; u_1 denotes the velocity amplitude; γ is the ratio of specific heats, which ranges from 1 to 5/3 for lossy isothermal refilling flows to adiabatic. We now choose to use the density ρ as a problem variable, rather than the temperature or scale height h .

Perturbing the quantities backward in time, $p = p_0 - p_1$ and $\rho = \rho_0 - \rho_1$, from a final equilibrium state (p_0, ρ_0) leaves the hydrostatic relation equation (9) with p_0 coupled to the magnetic field through the cross-field equation (11), and three coupled perturbative equations for (p_1, ρ_1, u_1)

$$\rho_0 \frac{\partial u_1}{\partial t} = \frac{\partial p_1}{\partial z} + \rho_1 g \cos \theta, \quad (\text{E.3})$$

$$\frac{\partial \rho_1}{\partial t} = \frac{\partial}{\partial z}(\rho_0 u_1), \quad (\text{E.4})$$

and $p_1 = \gamma(p_0/\rho_0)\rho_1$, introducing θ as the angle between the magnetic field direction z and the radial r . With small positive pressure and density deficits p_1 and ρ_1 , a small positive velocity

u_1 is required from equation (E.3) corresponding to an upward flow opposite the normal gravitational stratification. Refilling changes the gas-pressure profile, in effect heating the gas compressively.

The unperturbed density $\rho_0 = p_0/(gh)$, varies on a scale similar to the gas pressure p_0 , since the gravity g and temperature contained in h vary on much larger scales; thus the derivative is approximated $\partial \rho_0 / \partial z \rightarrow \rho_0 \cos \theta / h$. The perturbed quantities must vary on the scale of the magnetic field $2h / \cos \theta$, giving $\partial(p_1, u_1) / \partial z \rightarrow (p_1, u_1) \cos \theta / (2h)$. Substituting for the time derivative $\partial / \partial t \rightarrow 1 / \tau_u$ lets us solve for the hydrodynamic timescale

$$\tau_u = \frac{1}{\cos \theta} \left(\frac{h}{g} \frac{4}{6 + 3\gamma} \right)^{1/2}, \quad (\text{E.5})$$

which is proportional to the gravitational free-fall time through the scale height h . For a radial field $\theta = 0$, mixed lossy conditions $\gamma = 1.2$, and $h = r_\odot/(2\ell + 4)$, we obtain $\tau_{\text{hyd}} = 349$ s for solar surface conditions with $\ell = 2.33$, which is just over twice the magnetic adjustment time τ_B . The hydrodynamic adjustment time increases with more lossy conditions and smaller γ , but overall depends only weakly on the thermodynamics.

References

- Altschuler, M. D. & Newkirk, G. J. 1969, Magnetic Fields and the Solar Corona: III. Methods of Calculating Coronal Fields, *Solar Phys.*, 9, 131–149
- Anderson, S. W., Raymond, J. C., & van Ballegooijen, A. 1996, Ultraviolet Emission-Line Intensities and Coronal Heating by Velocity Filtration: Collisionless Results, *ApJ*, 457, 939–948
- Arendt, U. & Schindler, K. 1988, On the existence of three-dimensional magnetohydrostatic equilibria, *A&A*, 204, 229–234
- Ayres, T. R. 1981, Thermal bifurcation in the solar outer atmosphere, *ApJ*, 244, 1064–1071
- Bogdan, T. J. & Low, B. C. 1986, The three-dimensional structure of magnetostatic atmospheres. II - Modeling the large-scale corona, *ApJ*, 306, 271–283
- Carlsson, M. & Stein, R. F. 1995, Does a nonmagnetic solar chromosphere exist?, *ApJ*, 440, L29–L32
- Cauzzi, G., Falchi, A., Falciani, R., & Smaldone, L. A. 1996, Coordinated observations of solar activity phenomena. II. The velocity field pattern in an elementary flare., *A&A*, 306, 625–637
- Cheng, C. Z. & Choe, G. S. 1998, Current Sheets and Prominence Formation in the Solar Atmosphere, *ApJ*, 505, 376–389
- Coles, W. A. & Harmon, J. K. 1978, Interplanetary scintillation measurements of the electron density power spectrum in the solar wind, *J. Geophys. Res.*, 83, 1413–1420
- Craig, I. J. D. & Brown, J. C. 1976, Fundamental limitations of X-ray spectra as diagnostics of plasma temperature structure, *A&A*, 49, 239–250
- Davis, J. M., Gerassimenko, M., Krieger, A. S., & Vaiana, G. S. 1975, The interpretation of simultaneous soft X-ray

- spectroscopic and imaging observations of an active region, *Sol. Phys.*, 45, 393–410
- Dungey, J. W. 1953, A family of solutions of the magnetohydrostatic problem in a conducting atmosphere in a gravitational field, *MNRAS*, 113, 180–187
- Dungey, J. W. 1958, *Cosmic Electrodynamics*, Cambridge University Press
- Fontenla, J. M., Avrett, E. H., & Loeser, R. 1990, Energy balance in the solar transition region. I - Hydrostatic thermal models with ambipolar diffusion, *ApJ*, 355, 700–718
- Giovanelli, R. G. 1982, Sunspot geometry and pressure balance, *Solar Phys.*, 80, 21–31
- Giovanelli, R. G. & Jones, H. P. 1982, The three-dimensional structure of atmospheric magnetic fields in two active regions, *Solar Phys.*, 79, 267–278
- Guhathakurta, M., Rottman, G. J., Fisher, R. R., Orrall, F. Q., & Altrock, R. C. 1992, Coronal Density and Temperature Structure from Coordinated Observations Associated with the Total Solar Eclipse of 1988 March 18, *ApJ*, 388, 633–643
- Hammer, R. 1982, Energy Balance of Stellar Coronae. II. Effect of Coronal Heating, *ApJ*, 259, 779–
- Hearn, A. G. & Kuin, N. P. M. 1981, Coronal loops and the minimum flux corona theory, *A&A*, 98, 248–250
- Heyvaerts, J. & Priest, E. R. 1984, Coronal heating by reconnection in DC current systems - A theory based on Taylor's hypothesis, *A&A*, 137, 63–78
- Hudson, H. S. 1991, Solar flares, microflares, nanoflares, and coronal heating, *Sol. Phys.*, 133, 357–369
- Jarrett, A. H. & von Klüber, H. 1958, Interferometric Investigation of Emission Lines of the Solar Corona During the Total Solar Eclipse of 1958 October 12, *MNRAS*, 122, 223–238
- Lin, H., Penn, M. J., & Tomczyk, S. 2000, A New Precise Measurement of the Coronal Magnetic Field Strength, *ApJ*, 541, L83–L86
- Lin, J., Zhang, Z. D., Wang, Z., & Smartt, R. N. 1992, The morphological characteristics and cooling mechanisms of the post-flare loop system of April 28, 1980, *A&A*, 253, 557–560
- Low, B. C. 1975, Nonisothermal magnetostatic equilibria in a uniform gravity field. I - Mathematical formulation, *ApJ*, 197, 251–255
- Low, B. C. 1977, Evolving force-free magnetic fields. II - Stability of field configurations and the accompanying motion of the medium, *ApJ*, 217, 988–998
- Low, B. C. 1980, On magnetostatic equilibrium in a stratified atmosphere, *Solar Phys.*, 65, 147–165
- Low, B. C. 1985, Three-dimensional structures of magnetostatic atmospheres. I - Theory, *ApJ*, 293, 31–43
- Low, B. C. 1991, Three-dimensional structures of magnetostatic atmospheres. III - A general formulation, *ApJ*, 370, 427–434
- Low, B. C. 1992, Formation of electric-current sheets in the magnetostatic atmosphere, *A&A*, 253, 311–317
- MacQueen, R. M., Eddy, J. A., Gosling, J. T., Hildner, E., Munro, R. H., Newkirk, G. A. J., Poland, A. I., & Ross, C. L. 1974, The Outer Solar Corona as Observed from Skylab: Preliminary Results, *ApJ*, 187, L85–L88
- MacQueen, R. M., Sime, D. G., & Picat, J.-P. 1983, The Properties of Coronal Voids, *Solar Phys.*, 83, 103–114
- Menzel, D. H. 1968, A Magnetohydrostatic Model of the Solar Corona., *AJ*, 73, S71–S72
- Neukirch, T. 1997, Nonlinear self-consistent three-dimensional arcade-like solutions of the magnetohydrostatic equations., *A&A*, 325, 847–856
- Newkirk, G. J., Dupree, A., & Schmahl, E. 1970, Magnetic Fields and the Structure of the Solar Corona II: Observations of the 12 November 1966 Solar Corona, *Solar Phys.*, 15, 15–39
- November, L. J. & Koutchmy, S. 1996, White-Light Coronal Dark Threads and Density Fine Structure, *ApJ*, 466, 512–528
- Parker, E. N. 1960, The Hydrodynamic Theory of Solar Corpuscular Radiation and Stellar Winds., *ApJ*, 132, 821–866
- Parker, E. N. 1972, Topological Dissipation and the Small-Scale Fields in Turbulent Gases, *ApJ*, 174, 499–510
- Parker, E. N. 1979, *Cosmical Magnetic Fields: Their Origin and Their Activity*, Clarendon Press, Oxford
- Parker, E. N. 1987, Magnetic Reorientation and the Spontaneous Formation of Tangential Discontinuities in Deformed Magnetic Fields, *ApJ*, 318, 876–887
- Petschek, H. E. & Thorne, R. M. 1967, The Existence of Intermediate Waves in Neutral Sheets, *ApJ*, 147, 1157–1163
- Pneuman, G. W. & Kopp, R. A. 1978, Downflow in the supergranulation network and its implications for transition region models, *Solar Phys.*, 57, 49–64
- Priest, E. R. 1972, A modification and criticism of Petschek's mechanism, *MNRAS*, 159, 389–402
- Rosner, R., Tucker, W. H., & Vaiana, G. S. 1978, Dynamics of the quiescent solar corona, *ApJ*, 220, 643–645
- Schatten, K. H., Wilcox, J. M., & Ness, N. F. 1969, A Model of Interplanetary and Coronal Magnetic Fields, *Solar Phys.*, 6, 442–455
- Schmieder, B., Forbes, T. G., Malherbe, J. M., & Machado, M. E. 1987, Evidence for gentle chromospheric evaporation during the gradual phase of large solar flares, *ApJ*, 317, 956–963
- Scudder, J. D. 1992, On the causes of temperature change in inhomogeneous low-density astrophysical plasmas, *ApJ*, 398, 299–318
- Syrovatskii, S. I. 1981, Pinch Sheets and Reconnection in Astrophysics, *ARA&A*, 19, 163–229
- Vaiana, G. S. & Rosner, R. 1978, Recent advances in coronal physics, *ARA&A*, 16, 393–428
- Vaiana, G. S., Zombeck, M., Krieger, A. S., & Timothy, A. F. 1976, ATM observations - X-ray results, *Ap&SS*, 39, 75–101
- Vainshtein, S. I. & Parker, E. N. 1986, Magnetic nonequilibrium and current sheet formation, *ApJ*, 304, 821–827
- Van Ballegooijen, A. A. 1985, Electric currents in the solar corona and the existence of magnetostatic equilibrium, *ApJ*, 298, 421–430
- Vernazza, J. E., Avrett, E. H., & Loeser, R. 1981, Structure of the Chromosphere. III. Models of the EUV Brightness

- Components of the Quiet Sun, *ApJS*, 45, 635–725
- Wagner, W. J., Newkirk, G. J., & Schmidt, H. U. 1983, An Observation of Prominence Condensation out of a Coronal Void, *Solar Phys.*, 83, 115–119
- Williams, L. L. & Mullan, D. J. 1996, Correlating Coronal Temperature and Gravitational Potential: A Test of the Nonthermal Boundary Hypothesis, *ApJ*, 457, L95–L98
- Withbroe, G. L. 1975, The analysis of XUV emission lines, *Sol. Phys.*, 45, 301–317
- Woo, R., Armstrong, J. W., Bird, M., & Patzold, M. 1995, Fine scale structure in coronal streamers, *ApJ*, 449, L91–L94
- Zweibel, E. G. & Hundhausen, A. J. 1982, Magnetostatic Atmospheres: A Family of Isothermal Solutions, *Solar Phys.*, 76, 261–299